Mathematical Modeling of the Transport and Dissolution of Citrate-Stabilized Silver Nanoparticles in Porous Media

ARTICLE *in* ENVIRONMENTAL SCIENCE & TECHNOLOGY · JULY 2013

Impact Factor: 5.33 · DOI: 10.1021/es400692r · Source: PubMed

5 AUTHORS, INCLUDING:

Amir Taghavy
University of Massachusetts Dartmouth
9 PUBLICATIONS **48** CITATIONS
SEE PROFILE

Kurt D Pennell
Tufts University
171 PUBLICATIONS **3,475** CITATIONS
SEE PROFILE

Linda M Abriola
Tufts University
203 PUBLICATIONS **5,135** CITATIONS
SEE PROFILE

Environmental Science & Technology

Article

pubs.acs.org/est

Mathematical Modeling of the Transport and Dissolution of Citrate-Stabilized Silver Nanoparticles in Porous Media

Amir Taghavy,[†] Anjuliee Mittelman,[†] Yonggang Wang,[†] Kurt D. Pennell,[†] and Linda M. Abriola*[,†]

[†]Department of Civil and Environmental Engineering, Tufts University, 200 College Ave, Medford, Massachusetts 02155, United States

Supporting Information

ABSTRACT: A one-dimensional mathematical model is developed and implemented to describe the coupled transport of citrate-stabilized silver nanoparticles (nAg) and dissolved silver ions in porous media. This hybrid numerical simulator employs an Eulerian finite difference (FD) method to model the reactive transport of dissolved constituents and a Lagrangian (random-walk particle-tracking (RWPT)) approach to capture the transport and differential aging of nanoparticles. Model performance is demonstrated by comparison of simulations with data obtained from a series of nAg transport and dissolution column experiments. A three pore volume pulse of a citrate-stabilized nAg suspension (ca. 3 mg/L) was introduced into a 12 or 16 cm long column packed with water-saturated quartz sand at a pore-water velocity of ca. 7.6 m/day and pH 4 or 7. While low retention levels (ca.17%) and no dissolution were observed for the pH 7 column, analysis of column effluent samples for pH 4 conditions indicated that ca. 88% of the injected silver mass was retained in the column, while 6% was eluted as particles (nAg) and 6% as dissolved ions (Ag^+). Hybrid model simulations, employing a lumped nAg dissolution coefficient of $(3.45 \pm 0.35) \times 10^{-2}$/h, are shown to accurately capture measured nAg transport and Ag^+ release behavior. A model sensitivity analysis explores the influence of flow velocity and particle size on nAg transport and fate, indicating that as velocity and particle size decrease, nAg dissolution and Ag^+ transport processes increasingly dominate silver mobility.

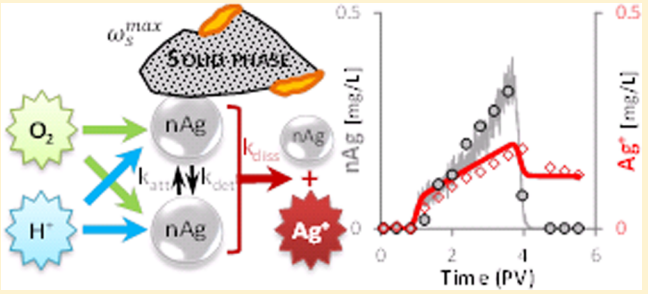

INTRODUCTION

Understanding the transport behavior and reactivity of nanoparticles (NPs) in porous media is essential for accurate assessment of their fate and potential influence on subsurface ecosystems and water supplies. Concerns over the potential adverse impacts of nAg on human health and the environment have arisen based upon widespread use in a variety of household products.[1] Although the risk posed by nAg to mammalian cells is currently unclear,[2,3] existing evidence suggests potential harm to organisms at lower ranks of the food chain. George et al.[2] reported multiple morphological and physiological effects on the development and hatching of nAg-treated zebra fish embryos. An understanding of nAg environmental fate is complicated by the coexistence of particulate (nAg) and ionic (Ag^+) forms, which likely exhibit different biological potency[4] and physiochemical and transport characteristics, and may exhibit independent or synergistic toxicity pathways.[5] nAg may undergo significant transformation by dissolution, which has been shown to be a cooperative oxidation process requiring both dissolved oxygen (DO) and protons.[6] nAg oxidation produces unstable peroxide intermediates, proceeding to complete reactive dissolution.[5] The biocidal activity of Ag^+ is substantially greater than that of nAg,[7] and thus, the extent and rate of dissolution will be of primary importance in assessing the environmental impacts of nAg releases. The following reaction stoichiometry has been proposed for the oxygen-mediated release of Ag^+ from nAg in the absence of other oxidants:[4,5]

$$2Ag_{(s)} + \frac{1}{2}0_{2(aq)} + 2H^+_{(aq)} \Leftrightarrow 2Ag^+_{(aq)} + H_20_{(l)} \quad (1)$$

Batch reactor studies have explored the influence of various factors, including solution pH,[5,8] temperature, natural organic matter,[5] electrolyte concentration, and ionic strength,[3] particle coating,[9,10] particle size,[4,11] and the oxidation state of silver[3] on the kinetics of ion release from nAg. A comprehensive assessment of nAg behavior in the subsurface, however, requires an understanding of nAg particle physical interactions with the porous matrix (i.e., transport and retention), coupled with knowledge of the dissolution process. Similar to other colloidal particles, the transport and retention of nAg is controlled by physicochemical properties and environmental conditions, such as flow velocity, soil grain size, and solution chemistry.[12] In addition, temporal changes in NP size and shape may influence nAg transport, retention, and dissolution

Received: February 16, 2013
Revised: June 27, 2013
Accepted: July 2, 2013
Published: July 2, 2013

Table 1. Summary of Experimental Properties and Model Input Parameters[a]

property	units	pH 7	pH 4 (1)	pH 4 (2)	pH 4 (3)	source/reference
column porosity		0.362	0.360	0.370	0.367	gravimetric measurement
column length	cm	16.0	12.0	12.1	16.0	gravimetric measurement
column internal diameter	cm	2.55	2.70	2.70	2.55	
column pore volume	mL	29.5	25.6	25.6	29.9	gravimetric measurement
Darcy velocity	m/day	2.81	2.52	2.52	2.81	gravimetric measurement
Peclet number		243	175	185	160	bromide tracer test
mean particle diameter (influent)	nm	11	12	12	12	DLS measurement
injected mass of silver	μg	275	243	234	228	ICP-OES
nAg pulse width	PV	3.02	3.08	2.88	3.04	gravimetric/ICP-OES
influent nAg conc.	mg/L	3.08	3.09	3.17	2.51	ICP-OES
Influent Ag^+ conc.	mg/L	0.01	0.05	0.06	0.05	ultrafiltration/ICP-OES
injected Ag mass	μg	269	243	234	214	
eluted Ag mass	μg	227	28	28	31	
retained Ag mass	μg	41	N/A	216	175	
experimental mass balance		97.5%	N/A	104.3%	96.5%	
attachment efficiency		1.20×10^{-3}	2.74×10^{-2}	3.22×10^{-2}	2.67×10^{-2}	Li et al.[18] model fit
retention capacity	μg/g	Inf.	8.51	3.91	2.80	Li et al.[18] model fit
contact efficiency (influent)		0.415	0.391	0.383	0.355	T&E correlation[21]
contact efficiency—diffusion		0.415	0.391	0.383	0.355	T&E correlation[21]
contact efficiency—interception		1.49×10^{-6}	1.98×10^{-6}	1.86×10^{-6}	1.87×10^{-6}	T&E correlation[21]
contact efficiency—gravity		1.41×10^{-5}	2.29×10^{-5}	2.29×10^{-5}	2.02×10^{-5}	T&E correlation[21]
contact efficiency (effluent)		0.415	0.3926	0.3842	0.3564	HELP-1D prediction
mean particle diameter (effluent)	nm	10	11.96	11.95	11.95	HELP-1D prediction
dissolution rate coefficient	1/h	N/A	3.86×10^{-2}	3.45×10^{-2}	3.16×10^{-2}	HELP-1D fit

[a]Single collector contact efficiency values were estimated from Tufenkji and Elimelech (T&E) correlation.[21]

behavior.[13] In contrast to nAg dissolution kinetics, there has been limited research on the transport of nAg.[14,15] This critical knowledge gap was identified in a recent review of environmental fate of nanomaterials.[16] Based upon a conceptual understanding of the processes controlling the environmental fate of nAg, mathematical models can be developed to represent the coupling of these processes, serving as effective tools for risk assessment and design of treatment or remediation strategies. Previous modeling attempts, however, have focused on either transport[10,15,17] or dissolution[4,5] of nAg in terrestrial systems. To the best of our knowledge, no prior study has explored the coupling of the chemical reactions and physical processes that simultaneously control the fate and transport of nAg in porous media. As stressed by Zhang et al.,[4] there is a clear need for better predictive models that link the ion release behavior of nAg to its environmental fate and transport.

To address these limitations, a one-dimensional Hybrid Eulerian-Lagrangian Particle (HELP-1D) model was developed to capture the coupled dissolution, transport, and retention processes that govern the fate of nAg in the subsurface. While prior NP transport modeling studies have assumed particle uniformity and stability during interactions with surfaces and with other reactive compounds,[12,18] the hybrid modeling approach, based on the numerical framework presented in Taghavy et al.,[19] can account for temporal and spatial changes in the physicochemical properties of nanoparticles subject to dissolution. HELP-1D was validated through comparisons with the experimental results of a nAg transport and dissolution column study. Batch experiments were used to assess the short-term dissolution kinetics of nAg on a time scale relevant to the column residence time. A model sensitivity analysis provided additional insight into the potential influence of flow velocity and particle size on the transport and dissolution of nAg particles.

MATHEMATICAL MODEL

The Transport of nAg and Dissolved Constituents. Two phases, aqueous and solid, are considered in the conceptual model of the porous medium. Consistent with the results of nonreactive tracer tests, the pore space is assumed to be fully accessible to aqueous phase flow. A general mass balance equation (i.e., transport equation) for component i can be expressed as shown:[19]

$$\frac{\partial}{\partial t}(\theta_w C_w^i + \rho_b \omega_s^i) + \frac{\partial}{\partial x}\left[\theta_w\left(C_w^i \nu_w - D_{wi}^h \frac{\partial C_w^i}{\partial x}\right)\right] = r^i \quad (2)$$

where subscript i denotes particulate and dissolved components (i.e., nAg, DO, and Ag^+), θ_w [−] is the volumetric water content, C_w^i (mol/m^3) is the molar concentration of component i in the aqueous phase, ρ_b [kg/m^3] is the bulk density of sand, and ω_s^i [mol/kg dry sand] is the molar concentration of component i associated with the sand grains per unit weight of the solid phase, ν_w (m/s) is the interstitial velocity of water, and D_{wi}^h (m^2/s) is hydrodynamic dispersion coefficient of component i in the aqueous phase. The reaction term r^i (mol/m^3 s) is the net molar rate of production of component i in the aqueous phase per unit bulk volume.

The retention of NPs in porous media is typically described by clean-bed colloid filtration theory (CFT).[15,18] Consistent with this theory, particles are deposited on the solid phase through the mechanisms of interception, diffusion, and sedimentation.[20] In the present work, a more general, modified version of colloid filtration theory (MFT) is implemented, which was developed and validated for transport of fullerene

dx.doi.org/10.1021/es400692r | Environ. Sci. Technol. 2013, 47, 8499−8507

nanoparticles (nC_{60}, dia ca. 95 nm) in water-saturated porous media.[18] The MFT model incorporates a maximum retention capacity and rate-limited attachment kinetics, as well as a first-order expression for particle detachment:

$$\frac{\rho b}{\theta_w}\frac{\partial \omega_s^{nP}}{\partial t} = k_{att}\psi_{att}C_w^{nP} - k_{det}\omega_s^{nP} \quad (3)$$

Here $\Psi_{att} = (1\text{-}\omega_s^{nP}/\omega_s^{nP,max})$ [−] is a site blocking function with $\omega_s^{nP,max}$ [mol/kg soil] as the particle retention capacity of the soil and k_{att} [s^{-1}] and k_{att} [s^{-1}] are the NP attachment and detachment rate coefficients, respectively. When $\Psi_{att} = 1$ (unlimited attachment capacity) and k_{det} is negligible, the model reduces to the classical CFT. Consistent with the CFT, the attachment rate coefficient is expressed as follows:[20]

$$k_{att} = \frac{3(1-\theta_w)\nu_w}{2d_c}\alpha_d\eta_0 \quad (4)$$

where d_c [m] is a representative collector (sand grain) diameter, the collision or attachment efficiency, α_d [−], represents the fraction of collisions that result in attachment of particles to the collector surface, and the single collector contact efficiency, η_0 [−], represents the frequency of particle collisions with the porous medium collector surfaces. The theoretical value of η_0 can be written as the sum of contributions from each collision mechanism (i.e., *Brownian* diffusion, interception, and gravitational sedimentation):[21]

$$\eta_0 = 2.4A_s^{1/3}N_R^{-0.081}N_{Pe}^{-0.715}N_{vdW}^{0.052} + 0.55A_sN_R^{1.675}N_A^{0.125} + 0.22N_R^{-0.24}N_G^{1.11} \quad (5)$$

Here, A_s [−], the *Happel* correction factor, is a porosity dependent parameter; $N_R = (d_p)/(d_c)$ [−] is the aspect ratio with d_p [m] being a representative particle diameter; $N_{Pe} = (U_w d_c)/(D_p)$ [−] is the Peclet number with U_w and $D_p = (k_BT)/(3\pi\mu d_p)$ representing the Darcy velocity and the diffusion coefficient of particles in an infinite medium, respectively; $N_{vdW} = (A)/(k_Bt)$ [−] is the *van der Waals* number, with A [J], k_B [J/K] and T [K] denoting the *Hamaker* constant, *Boltzman* constant, and temperature, respectively; $N_A = (A)/(3\pi\mu d_p^2U_w)$ [−] is the attraction number; and $N_G = (d_p/18)\ (\rho_p-\rho_w)g/(\mu_wU_w)$ is the gravity number, with μ[g m^{-1} s^{-1}], ρ_p [g m^{-3}], and ρ_w [g m^{-3}] representing the flowing phase dynamic viscosity, particle, and aqueous phase densities, respectively. Based on the values provided in Table 1, the overall *Hamaker* interaction parameter, A_{123}, for the attachment of nAg "1" onto a quartz sand surface "3" with water as the intervening medium "2" was estimated $A_{123} = A_{121}^{1/2}A_{323}^{1/2} = 5.36 \times 10^{-20}$ J with $A_{121} = 1.02 \times 10^{-20}$J[22] and $A_{323} = 28.2 \times 10^{-20}$J.[23] Although, Brownian diffusion is usually considered to be the dominant mechanism controlling the attachment of nanosized particles to collector surfaces,[24] for completeness, all three mechanisms are taken into account in eq 5 and are incorporated into the model (Supporting Information Figure S-3). Also note that η_0 is implicitly a function of particle size through its dependence on aspect ratio and Peclet, attraction, and gravity numbers.

nAg Dissolution. The nAg dissolution reaction is assumed to take place at the nanoparticle−water interface, where silver ions are then released into the bulk aqueous phase, thereby reducing the effective size of the nanoparticles. Consistent with the approach of Liu and Hurt,[5] nAg dissolution is represented using a first-order kinetic expression with respect to nAg concentration and the stoichiometric coefficients; $a_{Ag^+/nAg} = 1$ and $a_{DO/nAg} = 0.25$ (eq 1):

$$r^{nAg} = -k_{diss}(\theta_wC_w^{nAg} + \rho_b\omega_s^{nAg}) = -r^{Ag^+} = 0.25r^{DO} \quad (6)$$

Here $r^{Ag^+} = \partial/\partial t\ (\theta_wC_w^{Ag^+} + \rho_b\omega_s^{Ag^+})$, $r^{DO} = \partial/\partial t\ (\theta_wC_w^{DO})$ and $r^{nAg} = \partial/\partial t\ (\theta_wC_w^{nAg} + \rho_b\omega_s^{nAg})$ are the rate of change in concentrations of Ag^+, *D*O, and nAg per unit volume of porous medium. k_{diss} [s^{-1}] is the nAg dissolution rate coefficient, which is a function of the specific surface area (SSA) [m^2/g] of particles:

$$k_{diss}(x,t) = k_{diss}\cdot\frac{SSA(x,t)}{SSA_0} \quad (7)$$

where the subscript 0 refers to the system initial condition.

NUMERICAL IMPLEMENTATION

The HELP-1D transport simulator employed in this study is a modified version of an existing model, which was originally developed to simulate the transport of zerovalent iron nanoparticles reacting with halogenated organic compounds.[19] The reaction modules were refined to incorporate nAg dissolution, Ag^+ formation, and DO depletion. HELP-1D uses a Lagrangian random-walk particle-tracking approach to solve the transport and component interaction equations for the NPs, and a conventional Eulerian finite difference method is implemented to discretize reactive transport equations governing the dissolved species. Although each transport system is modeled independently, the RWPT and FD modules communicate via a message-passing module that transfers the reaction data through the sink/source term. HELP-1D tracks particle changes (mass, size, and surface area) for subpopulations of particles (herein called model particles) as dissolution proceeds and updates corresponding attachment and dissolution rate parameters. A flowchart illustrating the solution algorithm is included in the Supporting Information (Figure S-5).

Lagrangian Particle-Solid Phase interactions. The RWPT module distributes the nAg mass among discrete model particles, each of which representing a subpopulation (i.e., a binned collection) of actual nanoparticles. According to the RWPT method, the random path of a particle p, $x_p(t)$, is determined in discrete time steps Δt as[25]

$$x_p(t+\Delta t) = x_p(t) + u(x_p(t)t)\Delta t + Z\sqrt{2a_L|u(x_p(t),t)|\Delta t} \quad (8)$$

where Z [−] is a normally distributed random variable with average 0 and standard deviation 1, and u [m/s] is a corrected particle velocity expressed as follows:

$$u(xp(t),t) = v_w(x_p(t),t) + \frac{\partial D_{w_{nP}}^h}{\partial x} \quad (9)$$

To implement the transport equation (eqs 2 and 3) in the RWPT scheme, the attachment and detachment terms on the right-hand-side (RHS) of eq 3 are treated separately. In this approach, simultaneous capture and release processes are reduced to two successive attachment and detachment steps (principle of superposition). A capture probability is computed for all suspended model particles, and then a random chance is selected for each particle (a random number from a uniform distribution ranging between 0 and 1). Those particles whose

dx.doi.org/10.1021/es400692r | Environ. Sci. Technol. 2013, 47, 8499−8507

capture probability exceeds the random chance are marked as attached and fixed in their current position. The advection and dispersion terms on the left-hand-side (LHS) of eq 2 are computed using eqs 8 and 9. An expression is developed for capture probability, based upon the following relationship between aqueous and attached particle mass:

$$\frac{dC_w^{np}}{dt} + \frac{\rho_b}{\theta_w}\frac{d\omega_s^{np}}{dt} = 0 \tag{10}$$

Substituting the attachment term from eq 3 into eq 10 and rearranging terms, yields the following expression for the capture probability, P_p^{att} [−], of particle p

$$P_p^{att} = -\frac{dC_w^{np}}{C_w^{np}} \approx -\frac{\Delta C_w^{np}}{C_w^{np}} = k_{att}\psi_{att}\Delta t \tag{11}$$

The RHS term in eq 11 corresponds to the fraction of particles that are immobilized by deposition at the soil collector surfaces during a time increment, Δt.

The particle detachment process is modeled in an analogous way; a particle detachment probability, P_p^{det} [−], of particle p can be calculated from the following expression:

$$P_p^{det} = -\frac{d\omega_s^{np}}{\omega_s^{np}} \approx -\frac{\Delta\omega_s^{np}}{\omega_s^{np}} = k_{det}\Delta t \tag{12}$$

Particle-Dissolved Phase Interactions (i.e., nAg Dissolution). Chemical reactions are incorporated into the RWPT by assuming that, over a small time interval, Δt, the fractional change in the number of moles of Ag of each particle residing in a grid-block $((\Delta M_{p_i})/(M_{p_i}))$ can be approximated by the change in the average Ag-moles of all particles over that grid-block. That is

$$\forall_{i\in e}: \frac{\Delta M_{p_i}}{M_{p_i}} = \frac{\Delta(\sum_p^e M_p)}{\sum_p^e M_p} \tag{13}$$

where ΔM_{p_i} denotes the number of moles of Ag in particle i inside grid-block e. In a control volume, $\Delta V_e = A_c\Delta X^e$, where A_c [m^2] is the cross-sectional area and Δx^e [m] is the grid spacing at element e. The molar concentration of nAg particles in the aqueous phase can be defined as

$$C_w^{nAg}{}_e = \frac{\Sigma_p^e M_p}{\theta_{w_e}\Delta V_e} \tag{14}$$

Substituting eq 14 into eq 6, rearranging, and simplifying the terms assuming that $\theta_w^e\Delta V_e$ does not vary with time at a fixed position in space, yields:

$$\frac{dc_w^{nAg}}{c_w^{nAg}} = \frac{\Delta\left(\frac{\Sigma_p^e M_p}{\theta_{w_e}\Delta V_e}\right)}{\frac{\Sigma_p^e M_p}{\theta_{w_e}\Delta V_e}} = \frac{\Delta(\Sigma_p^e M_p)}{\Sigma_p^e M_p} = \frac{\Delta M_{p_i}}{M_{p_i}} = -k_{diss}\cdot\Delta t \tag{15}$$

Equation 15 can be used to calculate the change in Ag-content of each particle (i.e., $(\Delta M_{p_i})/(M_{p_i})$) during time step, Δt. The same approach was used to derive a similar expression for the retained particles.

As dissolution proceeds, the total surface area of nAg particles will decrease and the SSA will increase, resulting in differential dissolution rates for nAg particles based on their age and dissolution history. While conventional continuum-based transport models cannot capture changes in NP morphology, HELP-1D accounts for particle nonuniformity caused by dissolution by tracking the surface area of each simulated subpopulation of particles. The following expression is used to estimate the SSA of each model particle p, assuming that the particles remain spherical during dissolution:

$$SSA_p = \frac{SA_p}{V_p} = SSA_{p,0}\left(\frac{M_p}{M_{p,0}}\right)^{-1/3} \tag{16}$$

where SA_p[m^2] and V_p[m^3] are the surface area and volume of the particle p respectively. SSA_p is calculated from eq 16 and then incorporated into eq 7 to compute the particle-specific dissolution coefficient for each time step. After summing up the number of moles of Ag dissolved from all particles in each element e during time step Δt, the nAg dissolution information is conveyed as a source/sink term to the FD module to simulate reactive transport of DO and Ag^+:

$$r^{Ag^+}{}_e = -0.25r^{D0}{}_e = -\frac{\Sigma_p^e\Delta M_p}{\Delta V_e\Delta t} \tag{17}$$

MATERIALS AND METHODS

nAg Preparation and Analytical Methods. Citrate-stabilized nAg particles were prepared based on the method of Liu and Hurt[5] using sodium borohydride as the reducing agent and silver nitrate as the precursor. This method produced a 16 mg/L solution of nAg with a mean diameter of 12 ± 2 nm and nondetectable levels of silver ion (Ag^+). The particle size distribution (PSD) and zeta potential were obtained by dynamic light scattering (DLS) using a Zeta Sizer Nano (Malvern Instruments). Silver concentrations were quantified by inductively coupled plasma-optical emission spectrometry (ICP-OES 7300DV, Perkin-Elmer), which provided a linear response over the implemented concentration range of 0.05−3 mg/L. The method detection limit for silver ions by ICP-OES was 0.01 mg/L.[26] Silver ions were separated from the particulate form by centrifugation at 2800 × g for 20 min (Eppendorf) in 15 mL ultrafiltration units (Amicon Ultra 4, Millipore). Prior to analysis, solid samples were digested in concentrated nitric acid for 10 min at 190 °C using a CEM Discover SP-D microwave digester.

Batch Experiments. Silver ion release from nAg was monitored at pH 4 and 7 under oxygen-saturated conditions (ca. 8.9 mg/L O_2). Batch experiments were conducted in duplicate in glass bottles (Corning) and mixed continuously with a magnetic stir bar (700 rpm). Dissolved oxygen concentration was monitored using an oxygen-specific probe (LD0101 probe, Hach). All experiments were conducted with an initial total silver concentration of ca. 3 mg/L at room temperature (23 ± 1 °C) and with 10 mM $NaNO_3$ as the background electrolyte. Samples were collected every 20 minutes over a period of two hours and analyzed for total silver and dissolved silver. The mean particle size and zeta potential were also measured at each sampling event (Supporting Information Figure S-2).

Column Experiments. A series of four column experiments was conducted at either pH 4 or 7 under oxygen-saturated conditions (ca. 8.9 mg O_2/L) to measure the transport and dissolution of nAg. Glass chromatography columns (Kontes, 12 or 16 cm length × ca. 2.5 cm i.d.) were packed with acid washed 40−50 mesh Ottawa sand (sand grain density of 2.65

g/cm^3 and d_{50} = 360 μm) and saturated with a background electrolyte solution (10 mM $NaNO_3$) based on the methods of Wang et al.[27] Each experiment was conducted in a separate column packed with clean sand. Following a nonreactive tracer test (bromide), a three pore volume pulse of nAg suspension (ca. 3 mg/L) was introduced, followed by three pore volumes of nanoparticle-free solution. A peristaltic pump (Cole Palmer) was used to deliver both the feed solution and background electrolyte to the column in upflow mode at a flow rate of 1 mL/min. This flow rate corresponded to a pore-water velocity of ca. 7.6 m/d and yielded a column residence time of ca. 27 minutes. The pH of the background electrolyte feed solution and effluent samples were monitored over the course of the experiment (Supporting Information Figure S-1). The influent nAg suspension was sampled at the beginning and conclusion of the pulse injection and analyzed for total (nAg + Ag^+) and dissolved (Ag^+) phase silver. Effluent samples were collected continuously in 15 mL glass culture tubes (VWR) using a fraction collector (CF-2, Spectrum). Column effluent data were expressed as breakthrough curves (BTCs), where the concentration of nAg and Ag^+ was plotted against the number of dimensionless pore volumes (PV) delivered to the column.

RESULTS AND DISCUSSION

nAg Dissolution Kinetics. Formation of a small amount of Ag^+ ions (<0.02 mg/L) was observed in pH 7 batch reactors, whereas at pH 4 ca. 2.5% of the initial mass of silver had dissolved by the end the experiment (140 min) (Figure 1). For

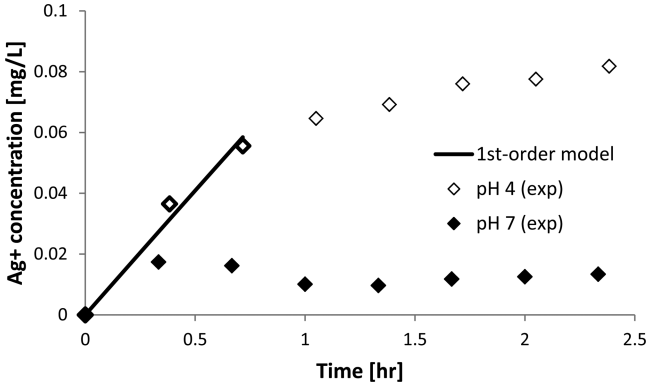

Figure 1. Dissolved silver ion concentrations measured in batch reactors as a function of pH and mixing time. First-order model (eq 6) fit obtained for pH 4 data set based on a LSSR procedure.

pH 4 the measured Ag^+ concentrations conformed to a hyper-exponential profile, indicating that a first-order kinetic model for citrate-stabilized nAg dissolution would not accurately describe the observed Ag^+ release rate. However, a first-order model with respect to nAg concentration was able to capture early time data, that is, the first 43 min of the experiment, consistent with residence time of the column (ca. 27 min). A least sum of squares residuals (LSSR) method yielded a dissolution rate constant of 0.0242 1/h at pH 4(r^2 = 0.98). This rate parameter is 2−3 times larger than the previously reported values of 0.01 1/h [5] and ca. 0.014 1/h,[4] measured at higher pH values of 5.6 and 5.67, respectively.

Simulation of Coupled nAg Transport and Dissolution. Effluent concentration data were obtained from four column experiments conducted to measure the transport of citrate-stabilized nAg and dissolved ions (Ag^+) in 40−50 mesh Ottawa sand at pH 7 and 4. A summary of column experimental conditions is presented in Table 1. At pH 7, ca. 83% of the injected nAg mass was recovered in column effluent samples in the form of particulate silver, with no detectable levels of Ag^+ (Figure 2). When the pH was reduced to 4,

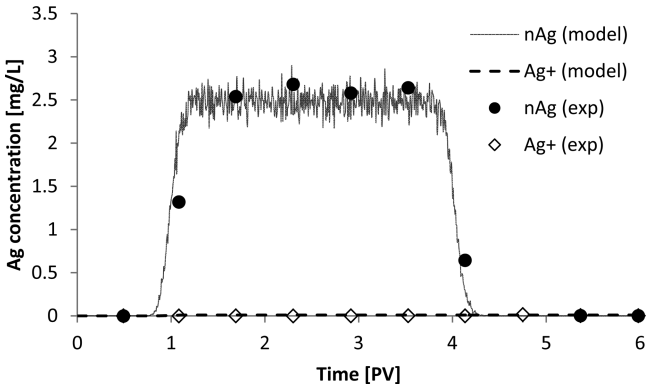

Figure 2. Measured and simulated effluent concentrations of nAg particles and Ag^+ ions at pH 7 performed in water-saturated column packed with 40−50 mesh Ottawa sand.

however, delayed breakthrough and lower maximum concentrations of nAg were observed in all three replicate columns (Figure 3). Substantially reduced mobility of nAg particles was observed, with only about 6% of the injected nAg mass recovered in effluent samples as nanoscale silver particles (An additional 6% was recovered as dissolved ion (Ag^+)).

To estimate the deposition parameters appropriate to these column experiments, a single equation Eulerian nanoparticle transport model,[18] based on the MFT model, was fit to experimental nAg effluent data using the LSSR method. This approach was used since direct application of HELP-1D to inverse problems is hindered by the stochastic oscillations around the expected value inherent in the RWPT scheme. Figures 2 and 3(a) present a comparison of HELP-1D simulations, using these fitted parameters, with measured nAg effluent concentration data at pH 7 and pH 4, respectively. Inspection of these figures reveals that the shape of the nAg breakthrough curve at pH 7 (Figure 2) is consistent with CFT model predictions (symmetric curve with a plateau region), while an MFT modeling approach is necessary to accurately represent effluent data obtained from pH 4 experiments (Figure 3). A single-collector attachment efficiency of 1.20×10^{-3} provided the best fit to pH 7 effluent data; at pH 4, the estimated attachment efficiencies were ca. 20 times higher, with a mean value of $(2.88 \pm 0.27) \times 10^{-2}$. The fitted maximum retention capacity ($\omega_s^{nP,max}$) was 5.07 ± 2.86 μg/g at pH 4. The higher affinity of nAg for the sand surface at pH 4 is consistent with calculated DLVO interaction energy profiles (Supporting Information Figure S-4).

At pH 7, very low concentrations of Ag^+ (<0.015 mg/L) were detected in effluent samples, consistent with the minimal nAg dissolution observed in the batch experiments. Given this absence of significant dissolution, a traditional CFT model[20] is able to capture the measured transport behavior for total silver under these conditions. Due to the significant dissolution of nAg at pH 4, however, a coupled transport/dissolution modeling approach is required. Figure 3(b) provides a comparison of HELP-1D model simulations for Ag^+ breakthrough with data obtained from the column experiments

dx.doi.org/10.1021/es400692r | Environ. Sci. Technol. 2013, 47, 8499−8507

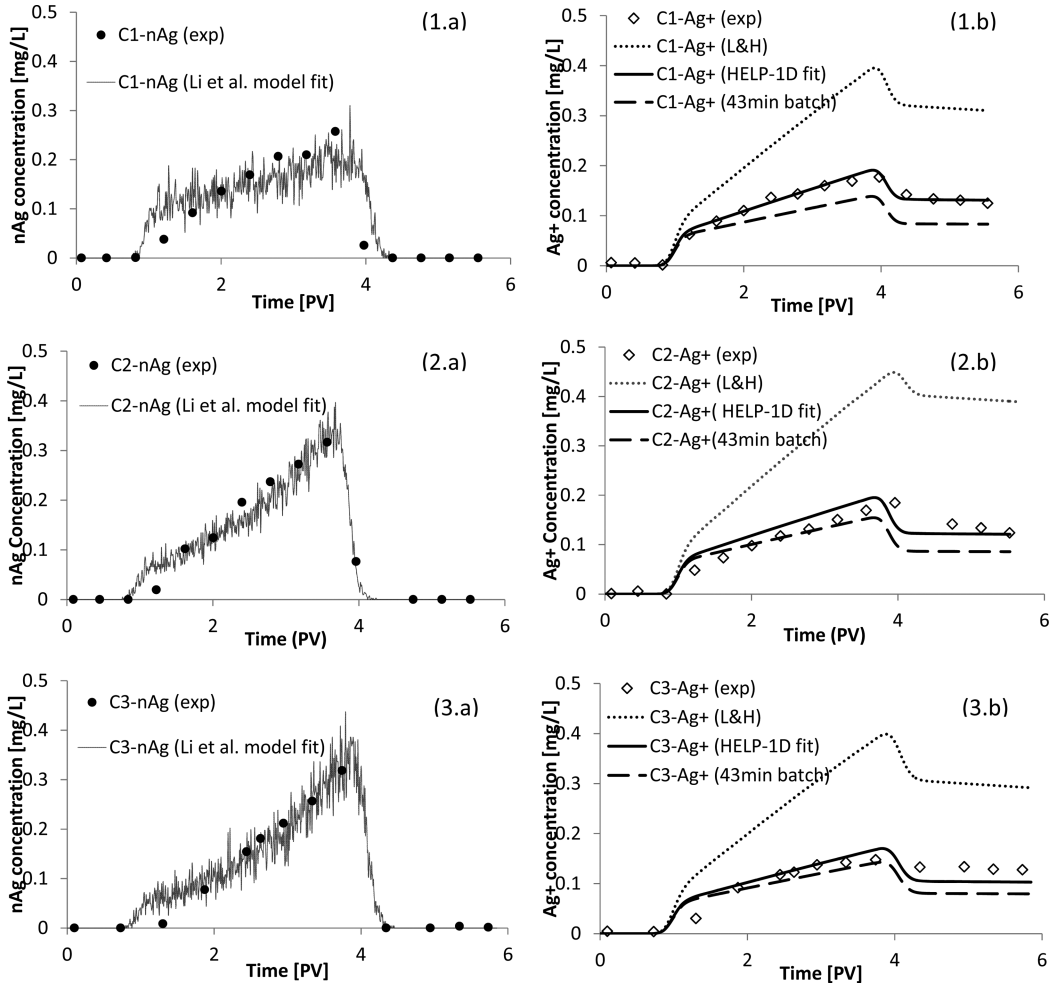

Figure 3. Measured and simulated effluent concentrations of (a) nAg particles and (b) Ag^+ ions in water-saturated column experiments (1, 2, 3) conducted at pH 4.

conducted at pH 4. Model input parameters are provided in Table 1.

Inspection of Figure 3(b) reveals that the hybrid model successfully captures the observed trends in Ag^+ release under dynamic flow conditions. Here, an nAg dissolution rate constant (k_{diss}) was fit to reproduce each of the Ag^+ effluent BTCs. The mean dissolution rate constant obtained from the three pH 4 columns was $(3.49 \pm 0.35) \times 10^{-2}$ 1/h. While the fitted rate constants from column experiments are of the same magnitude, they are approximately 1.4-times larger than the batch determined rate constant (i.e., 2.42×10^{-2} 1/h). This discrepancy can be attributed to different mixing conditions between the column and batch systems and the higher overall oxygen to silver molar ratio in the column. In addition, a higher column-based dissolution constant is consistent with the smaller residence time in the columns (ca. 27 min) compared to the time interval (ca. 43 min) over which the batch-based constant was determined. Liu and Hurt[5] presented a batch-derived empirical correlation to estimate the rate of nAg dissolution as a function of a number of physicochemical characteristics of the aqueous medium including temperature and pH. For the conditions in the present study, this correlation yields a dissolution rate constant of 9.62×10^{-2} 1/h, which is approximately 3 times larger than the value measured in the batch reactors. This discrepancy is consistent with the smaller size of the nAg particles used by Liu and Hurt (ca. 5 nm versus ca. 12 nm diameter), which would possess approximately 2.5 times greater surface area, assuming similar particle geometries. In addition, Liu and Hurt used a significantly lower initial concentration of nAg (0.05 mg/L) compared to the value employed herein (ca. 3 mg/L). Liu and Hurt observed a decrease in the dissolution rate constant (from 3.67×10^{-2} to 2.21×10^{-2} 1/h) with increasing total silver concentration (from 0.05 to 0.2 mg/L) at pH 5.6.

Based upon the fitted dissolution rate parameters, the HELP-1D model predicted that ca. 1.3% of the Ag mass dissolved during transport through the column at pH 4. This dissolution resulted in a slight reduction in the mean diameter of particles, from 12 nm (influent) to ca. 11.95 nm (effluent). The corresponding reduction in nAg size was associated with a 0.3−0.35% increase in the single collector contact efficiency (η_0) of eluting particles (Table 1). For the solution conditions and residence time of the column transport experiments (ca. 2.5 h), the DLS-based PSD measurements indicated no discernible change in the mean diameter of nAg particles (ca. 11 nm at pH 7 and ca. 12 nm at pH 4) (Supporting Information Figure S-2). Therefore, the influence of particle aggregation on the transport and dissolution of nAg was not considered further in this work.

Model Sensitivity Analysis. A model sensitivity analysis was undertaken to explore the potential effects of flow velocity and particle size on the transport and dissolution of nAg particles. Several model outputs were examined, including the

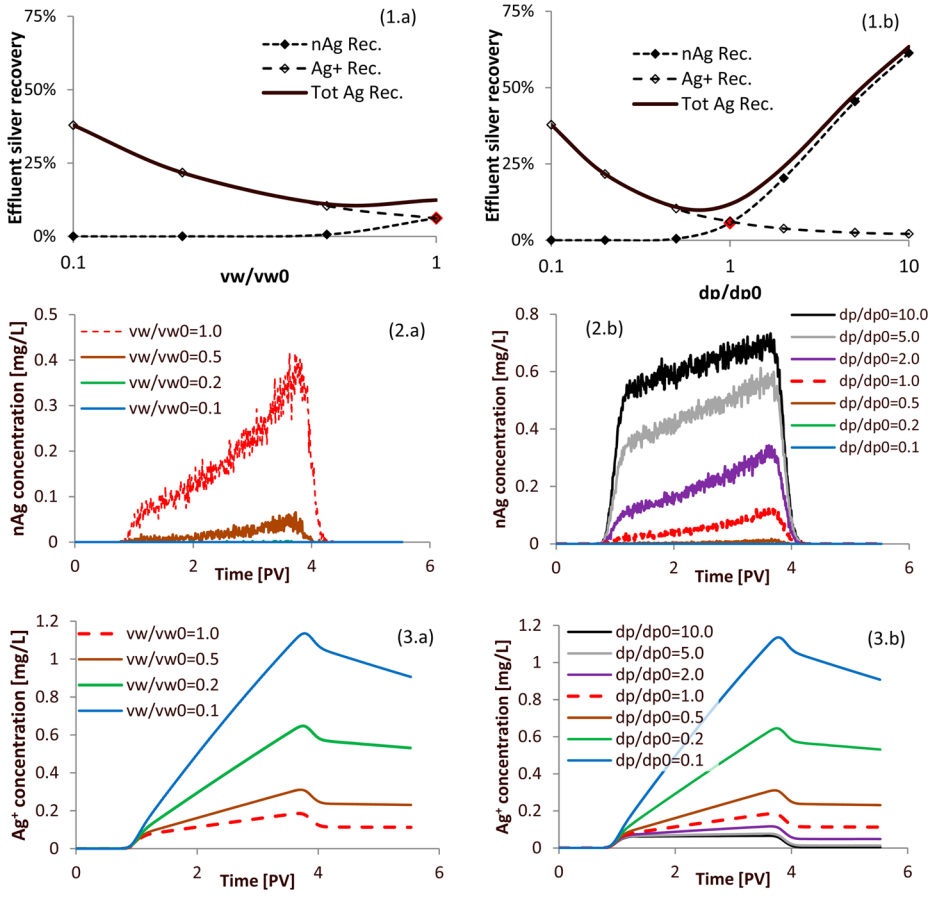

Figure 4. Influence of (a) applied flow rate (0.1 to 1.0 mL/min) (v_{w0} = 2.52 m/day at the flow rate of 1.0 mL/min) and (b) nanoparticle diameter (1.2−120 nm) (d_{p0} = 12 nm) on (1) total Ag recovery and on effluent concentrations of (2) nAg and (3) Ag^+ in water-saturated 40−50 mesh Ottawa sand at pH 4.

percent recovery of nAg, Ag^+, and total Ag in the column effluent. Only pH 4 data were utilized in this sensitivity study due to the relatively negligible nAg dissolution observed in the batch system at pH 7, which precluded estimation of a dissolution rate constant (see Figure 1).

Sensitivity to Flow Rate. The applied experimental volumetric flow rate resulted in a pore water velocity of ca. 7.6 m/day, several times larger than typical groundwater velocities (e.g., 0.15−1.4 m/day in shallow sandy aquifers[28]). Thus, sensitivity of the model output was evaluated over a one order-of-magnitude range lower than the experimental flow (i.e., from 0.1 to 1.0 mL/min). Here, it was assumed that the nAg dissolution rate constant did not vary over the range of flow velocities considered. The attachment efficiency (α_d) of nAg particles was also assumed independent of velocity (i.e., influenced only by chemical factors), consistent with filtration theory[20,29,30]. Model simulations suggest that, for identical volumes of nAg injection and background solution flushing, nAg recovery will decrease (from 6% to 0%) and Ag^+ recovery will increase (from 6% to 38%) with an order of magnitude reduction in flow rate (Figure 4(a)). Although a 2-fold decrease in flow rate slightly reduced the total Ag elution (from 12% to 10%), when expressed in terms of total Ag recovery, further reductions in flow rate (one order of magnitude) resulted in a substantial enhancement in the total silver recovery (from 12% to 38%). This behavior, which has been experimentally observed by other investigators,[14] can be explained by the dependence of nAg retention on flow rate. As the flow rate decreases, the single collector contact efficiency (η_0) increases, resulting in enhanced retention of nAg particles. For identical injection volumes, particle residence time increases as flow velocity decreases, with a corresponding enhancement in nAg dissolution. The results of this sensitivity analysis indicate that seepage velocity will have a pronounced effect on the transport and dissolution of citrate-stabilized nAg under typical groundwater flow conditions.

Sensitivity to Nanoparticle Size. A number of factors, including the method of production, nAg dissolution, and ionic strength, influence the size of nAg particles in aqueous suspension. The measured mean particle diameter in this study was ca. 12 nm, whereas nAg sizes reported in the literature range from less than 10 nm[5,31] to greater than 100 nm.[32,33] For this sensitivity analysis, the initial mean particle diameter was varied over two orders-of-magnitude, from 1.2 to 120 nm and particle attachment efficiency (α_d) and SSA-normalized nAg dissolution constant were assumed independent of nanoparticle size. With a 10-fold increase in particle size, the model predicts an overall increase in total Ag recovery from 12% to 63%, which can be attributed to enhanced particle mobility (Figure 4(b)). This behavior is a consequence of eq 5, which estimates a lower single collector contact efficiency value for nAg with an increase in primary particle diameter from 12 to 120 nm. Note that enhanced recovery occurs even though the recovery of Ag^+ decreases from 6% to 2%, due to the lower SSA of the larger particles. A 10-fold decrease in particle size also enhanced total Ag recovery from 12% to 38%. This trend

dx.doi.org/10.1021/es400692r | Environ. Sci. Technol. 2013, 47, 8499−8507

was attributed to an increase in nAg dissolution associated with the higher SSA of the smaller particles. Simulations predicted complete retention of particles smaller than 6 nm, resulting from the strong influence of Brownian diffusion, suggesting that oxidative dissolution would be the governing mechanism for Ag transport for very small particles. This is in agreement with previous studies that observed that citrate-stabilized nAg is not persistent as a particle in aquatic environments.[5]

Findings of this study demonstrate the importance of accounting for nAg dissolution in the integrated assessment of nAg fate in terrestrial environments. Simulations conducted with the hybrid Eulerian-Lagrangian model were able to capture the observed transport trends of both particulate and dissolved forms of silver. HELP-1D provides a modeling framework that can be used to simulate the reactive transport of other NPs that exhibit nonuniform physicochemical characteristics or NPs that experience a transformation of properties based on particle-specific and/or path-specific migration in porous media.

■ ASSOCIATED CONTENT

Supporting Information

Additional information as noted in the text. This material is available free of charge via the Internet at http://pubs.acs.org.

■ AUTHOR INFORMATION

Corresponding Author

*E-mail: linda.abriola@tufts.edu.

Notes

The authors declare no competing financial interest.

■ ACKNOWLEDGMENTS

We thank Mr. Matthew D. Becker for assistance with the simulation of nAg transport column experiments. Support for this research was provided by a grant from the National Science Foundation, Award no. CBET-0854136. The work has not been subject to NSF review, and therefore, does not necessarily reflect the views of the organization and no official endorsement should be inferred.

■ REFERENCES

(1) Wiesner, M. R.; Lowry, G. V.; Alvarez, P.; Dionysiou, D.; Biswas, P. Assessing the risks of manufactured nanomaterials. *Environ. Sci. Technol.* **2006**, *40* (14), 4336−4345.

(2) George, S.; Xia, T.; Rallo, R.; Zhao, Y.; Ji, Z.; Lin, S.; Wang, X.; Zhang, H.; France, B.; Schoenfeld, D.; Damoiseaux, R.; Liu, R.; Lin, S.; Bradley, K. a.; Cohen, Y.; Nel, A. E. Use of a high-throughput screening approach coupled with in vivo zebrafish embryo screening to develop hazard ranking for engineered nanomaterials. *ACS Nano* **2011**, *5*, 1805−17.

(3) Li, X.; Lenhart, J. J.; Walker, H. W. Dissolution-accompanied aggregation kinetics of silver nanoparticles. *Langmuir* **2010**, *26* (22), 16690−16698.

(4) Zhang, W.; Yao, Y.; Sullivan, N.; Chen, Y. Modeling the primary size effects of citrate-coated silver nanoparticles on their ion release kinetics. *Environ. Sci. Technol.* **2011**, *45*, 4422−8.

(5) Liu, J.; Hurt, R. H. Ion release kinetics and particle persistence in aqueous nano-silver colloids. *Environ. Sci. Technol.* **2010**, *44*, 2169−75.

(6) Kent, R. D.; Vikesland, P. J. Controlled evaluation of silver nanoparticle dissolution using atomic force microscopy. *Environ. Sci. Technol.* **2011**, *46* (13), 6977−6984.

(7) Sotiriou, G. A.; Pratsinis, S. E. Antibacterial activity of nanosilver ions and particles. *Environ. Sci. Technol.* **2010**, *44* (14), 5649−5654.

(8) Elzey, S.; Grassian, V. H. Agglomeration, isolation and dissolution of commercially manufactured silver nanoparticles in aqueous environments. *J. Nanopart. Res.* **2009**, *12*, 1945−1958.

(9) Zook, J. M.; Halter, M. D.; Cleveland, D.; Long, S. E., Disentangling the effects of polymer coatings on silver nanoparticle agglomeration, dissolution, and toxicity to determine mechanisms of nanotoxicity. *J. Nanopart. Res.* **2012**, *14*, (10).

(10) Song, J. E.; Phenrat, T.; Marinakos, S.; Xiao, Y.; Liu, J.; Wiesner, M. R.; Tilton, R. D.; Lowry, G. V. Hydrophobic interactions increase attachment of gum arabic-and PVP-coated Ag nanoparticles to hydrophobic surfaces. *Environ. Sci. Technol.* **2011**, *45* (14), 5988−5995.

(11) Sotiriou, G. A.; Meyer, A.; Knijnenburg, J. T. N.; Panke, S.; Pratsinis, S. E. Quantifying the origin of released Ag+ ions from nanosilver. *Langmuir* **2012**, *28* (45), 15929−15936.

(12) Torkzaban, S.; Kim, Y.; Mulvihill, M.; Wan, J.; Tokunaga, T. K. Transport and deposition of functionalized CdTe nanoparticles in saturated porous media. *J. Contam. Hydrol.* **2010**, *118*, 208−17.

(13) Lin, D.; Tian, X.; Wu, F.; Xing, B. Fate and transport of engineered nanomaterials in the environment. *J. Environ. Qual.* **2010**, *39*, 1896.

(14) Sagee, O.; Dror, I.; Berkowitz, B. Transport of silver nanoparticles (AgNPs) in soil. *Chemosphere* **2012**, *88*, 670−675.

(15) Tian, Y.; Gao, B.; Silvera-Batista, C.; Ziegler, K. J. Transport of engineered nanoparticles in saturated porous media. *J. Nanopart. Res.* **2010**, *12*, 2371−2380.

(16) Peralta-Videa, J. R.; Zhao, L.; Lopez-Moreno, M. L.; de la Rosa, G.; Hong, J.; Gardea-Torresdey, J. L. Nanomaterials and the environment: A review for the biennium 2008−2010. *J. Hazard. Mater.* **2011**, *186*, 1−15.

(17) Lin, S.; Cheng, Y.; Bobcombe, Y. L.; Jones, K.; Liu, J.; Wiesner, M. R. Deposition of silver nanoparticles in geochemically heterogeneous porous media: Predicting affinity from surface composition analysis. *Environ. Sci. Technol.* **2011**, *45* (12), 5209−5215.

(18) Li, Y.; Wang, Y.; Pennell, K. D.; Abriola, L. M. Investigation of the transport and deposition of fullerene (C60) nanoparticles in quartz sands under varying flow conditions. *Environ. Sci. Technol.* **2008**, *42*, 7174−80.

(19) Taghavy, A.; Costanza, J.; Pennell, K. D.; Abriola, L. M. Effectiveness of nanoscale zero-valent iron for treatment of a PCE−DNAPL source zone. *J. Contam. Hydrol.* **2010**, *118* (3−4), 128−142.

(20) Yao, K.-m.; Habibian, M. T.; O'Meila, C. R. Water and waste water filtration: Concepts and applications. *Environ. Eng. Sci.* **1971**, *5*, 1105−1112.

(21) Tufenkji, N.; Elimelech, M. Correlation equation for predicting single-collector efficiency in physicochemical filtration in saturated porous media. *Environ. Sci. Technol.* **2004**, *38*, 529−36.

(22) Bergstrom, L. Hamaker constants of inorganic materials. *Adv. Colloid Interface Sci.* **1997**, *70*, 125−169.

(23) Israelechvili, J. *Intermolecular and Surface Forces*, 2 ed.; Academic Press: London, 1992.

(24) Petosa, A. R.; Jaisi, D. P.; Quevedo, I. R.; Elimelech, M.; Tufenkji, N. Aggregation and deposition of engineered nanomaterials in aquatic environments: Role of physicochemical interactions. *Environ. Sci. Technol.* **2010**, *44*, 6532−49.

(25) Kinzelbach, W., *Groundwater Modeling: An Introduction with Sample Programs in Basic*; Elsevier: Amsterdam, 1986.

(26) Hubaux, A.; Vos, G. Decision and detection limits for calibration curves. *Anal. Chem.* **1970**, *42* (8), 849−855.

(27) Wang, Y.; Li, Y.; Fortner, J. D.; Hughes, J. B.; Abriola, L. M.; Pennell, K. D. Transport and retention of nanoscale C60 aggregates in water-saturated porous media. *Environ. Sci. Technol.* **2008**, *42*, 3588−94.

(28) Kunkel, R.; Wendland, F. WEKU − a GIS-Supported stochastic model of groundwater residence times in upper aquifers for the supraregional groundwater management. *Environ. Geol.* **1997**, *30* (1−2), 1−9.

(29) Elimelech, M.; O'Meila, C. R. Kinetics of deposition of colloidal particles in porous media. *Environ. Eng. Sci.* **1990**, *24*, 1528−1536.

(30) Elimelech, M.; Gregory, J.; Jia, X.; WIlliams, R. A. *Particle Deposition and Aggregation - Measurement, Modelling and Simulation*; Elsevier: Amsterdam, 1995.
(31) Damm, C.; Münstedt, H. Kinetic aspects of the silver ion release from antimicrobial polyamide/silver nanocomposites. *Appl. Phys. A: Mater. Sci. Process.* **2008**, *91*, 479−486.
(32) Benn, T. M.; Westerhoff, P. Nanoparticle silver released into water from commercially available sock fabrics. *Environ. Sci. Technol.* **2008**, *42*, 4133−9.
(33) Geranio, L.; Heuberger, M.; Nowack, B. The behavior of silver nanotextiles during washing. *Environ. Sci. Technol.* **2009**, *43*, 8113−8.